Supporting Information

Highly Efficient and Sustainable Non-Precious-Metal Fe−N−C Electrocatalysts for Oxygen Reduction Reaction

Meng Sun[†], *Douglas Davenport*[†], *Huijuan Liu*[‡], *Jiuhui Qu**[‡], *Menachem Elimelech*[†], *and Jinghong Li**[§]

[†] Department of Chemical and Environmental Engineering, Yale University, New Haven, Connecticut 06511, United States.

[‡] School of Environment, Tsinghua University, Beijing 100084, China.

[§] Department of Chemistry, Beijing Key Laboratory for Microanalytical Methods and Instrumentation, Tsinghua University, Beijing 100084, China.

***Corresponding author**

Tel.: +86-10-62849151; fax: +86-10-6292355; E-mail: jhqu@tsinghua.edu.cn (J. Qu)

Tel and Fax: +86-10-62795290; E-mail: jhli@mail.tsinghua.edu.cn (J. Li)

Supporting Materials Contents

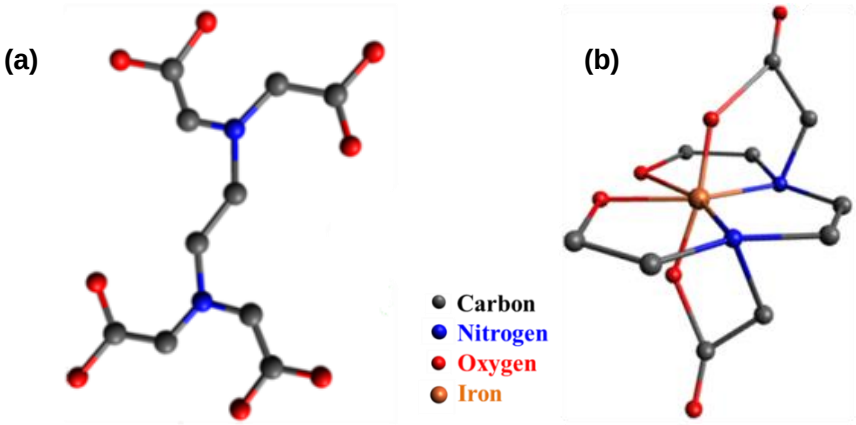

Figure S1. Molecular structure of (a) EDTA and (b) EDTA−Fe.

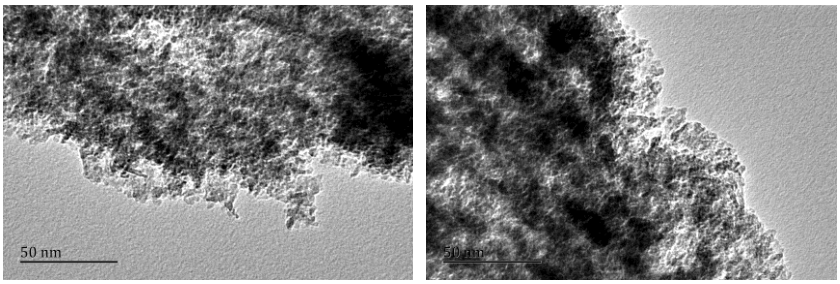

Figure S2. The TEM images of as-prepared Fe−N−C−700 catalysts.

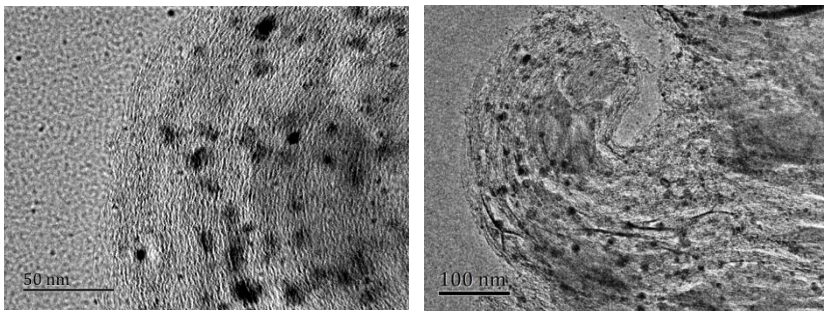

Figure S3. The TEM images of as-prepared Fe−N−C−900 catalysts.

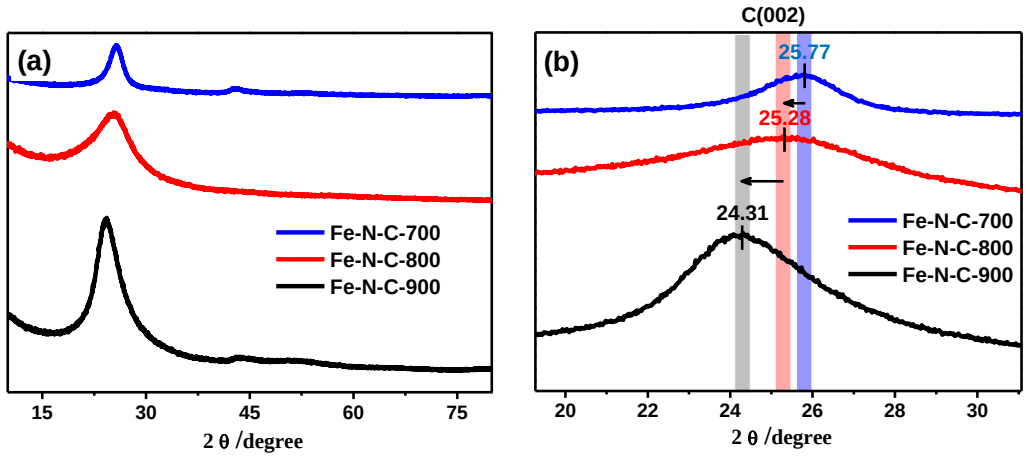

Figure S4. (a) The X-ray diffraction (XRD) patterns of as-prepared Fe−N−C−700, Fe−N−C−800 and Fe−N−C−900 catalysts. (b) The typical diffraction peak of (002) facet of graphite carbon on Fe−N−C−700, Fe−N−C−800 and Fe−N−C−900 catalysts

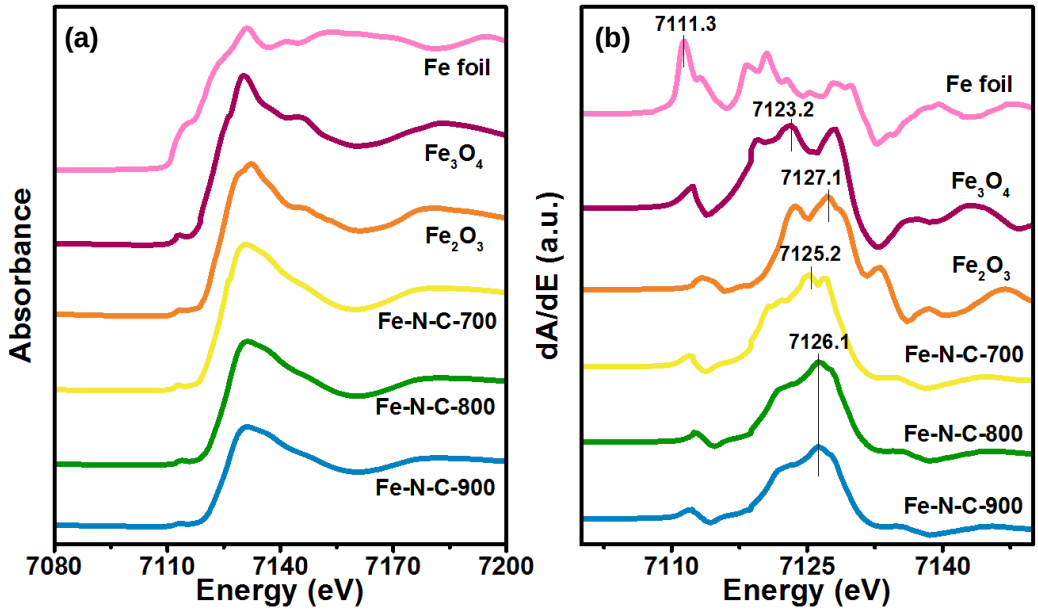

Figure S5. (a) Normalized XANES and (b) first-order derivate of XANES of Fe K-edge of Fe−N−C−700, Fe−N−C−800, Fe−N−C−900, and Fe reference samples

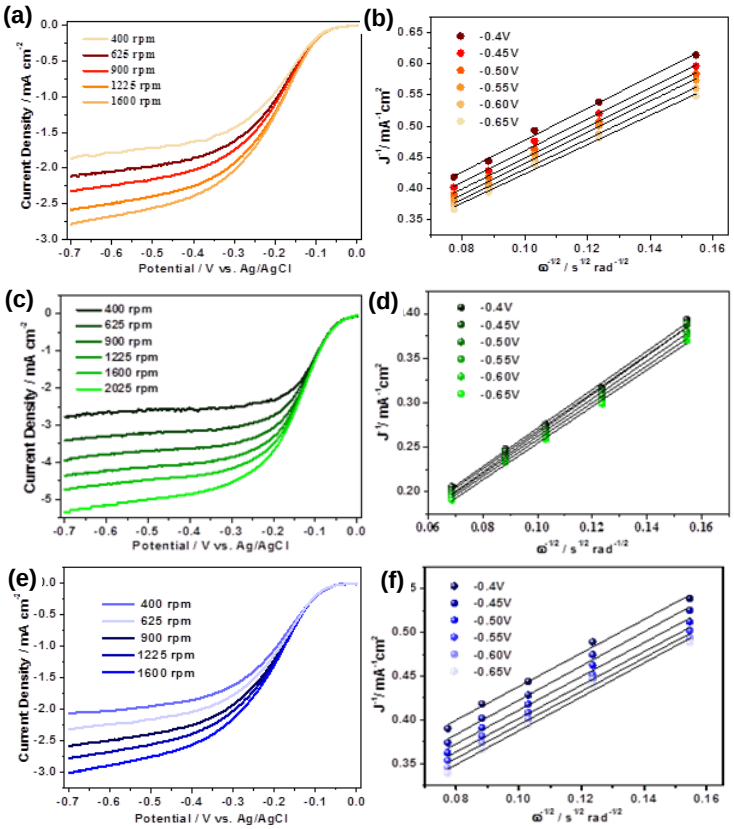

Figure S6. RDE curves of (a) Fe−N−C−700, (c) Fe−N−C−800 and (e) Fe−N−C−900 in O_2-saturated 0.1 M KOH solution at various rotation rates range from 400 to 2025 rpm. Sweep rate: 5 mV·s^{-1}. The corresponding K-L plot of (b) Fe−N−C−700, (d) Fe−N−C−800 and (f) Fe−N−C−900 derived from different potential from -0.4 to -0.65 V.

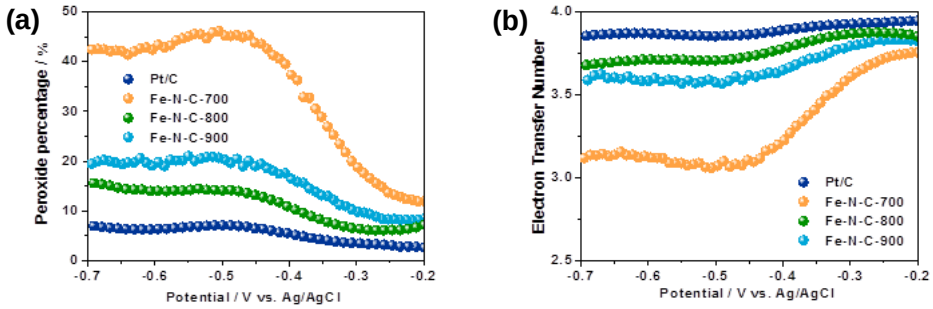

Figure S7. Changes of peroxide hydrogen generation and electron transfer number of of Pt/C, Fe−N−C−700, Fe−N−C−800 and Fe−N−C−900 calculated from the RRDE. The experiments were carried out in the O_2-saturated 0.1 M KOH solution, scan rate: 5 mV·s^{-1}, rotating speed: 1600 rpm

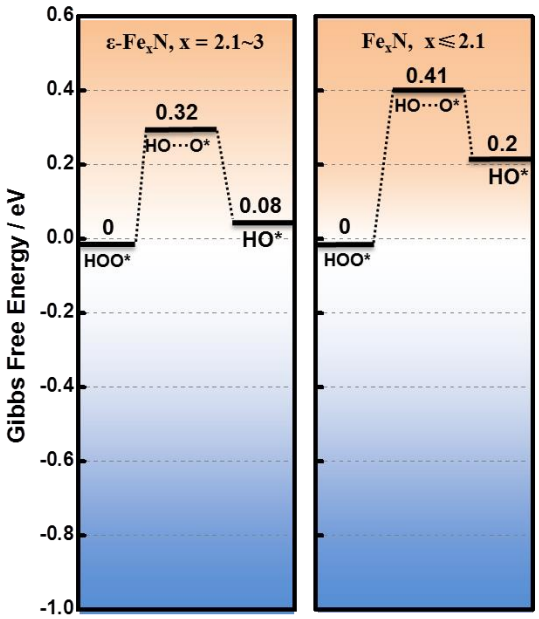

Figure S8. Free energy versus the critical reaction steps of the dissociation of O* from HOO* to HO* with the intermediate state of HO··O* on ε-Fe_xN and Fe_xN, structures identified on Fe−N−C catalysts.

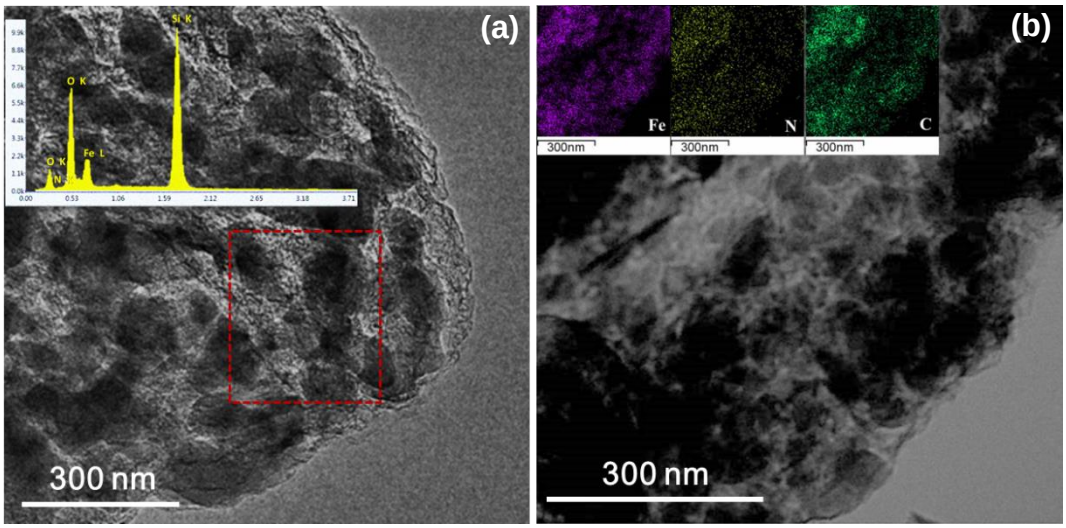

Figure S9. (a) TEM images of the Fe−N−C samples pyrolyzed from EDDA−Fe(II), and (b) HAADF-STEM images of as-synthesized Fe−N−C−800 catalysts from phenanthroline−Fe(II) precursor; the insets show the corresponding EDX and elemental mappings results, respectively.

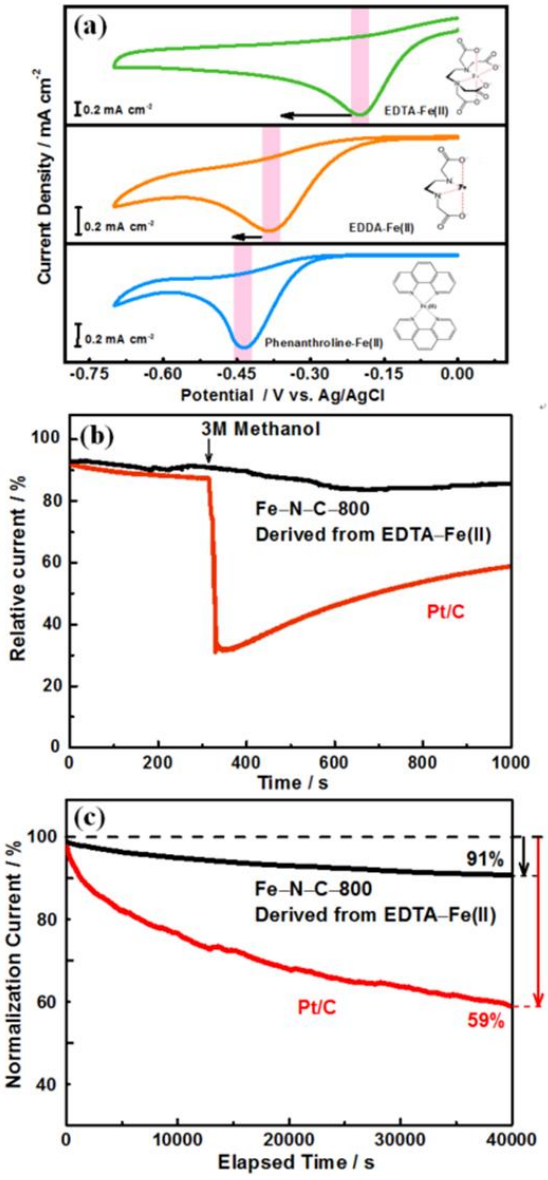

Figure S10. (a) CV curves of the Fe−N−C samples synthesized from EDTA−Fe(II), EDDA−Fe(II), and phenanthroline−Fe(II). (b) The current-time responses of the Fe−N−C−800 and Pt/C at -0.2 V in O_2-saturated 0.1 M KOH solution with a rotation rate of 1600 rpm for 1,000 s, and with the addition of 3 M methanol at around 300 s; (c) The current-time responses of the Fe−N−C−800 and Pt/C during a long elapsed time of 40,000 s. The rotating rate was set up to1600 rpm.

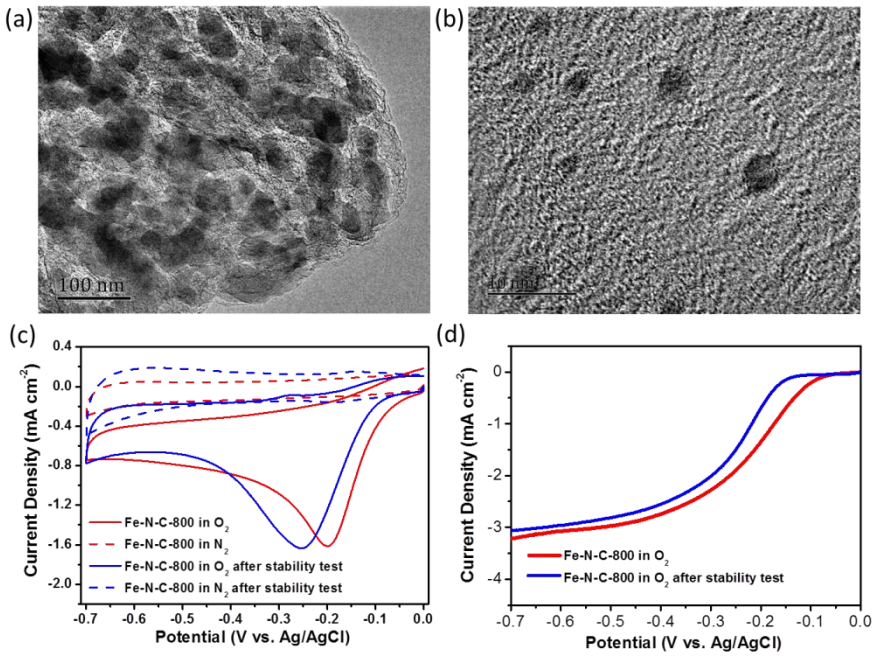

Figure S11. (a) (b) Morphological and structural evolution, (c) CV curves, and (d) LSV curves of the Fe−N−C−800 after long-term electrocatalytic ORR stability test for 40,000 s. CV curves were collected in O_2- and N_2-saturated 0.1 M KOH solution with a sweep rate of 5 mV s^{-1}. LSV curves were collected in O_2-saturated 0.1 M KOH solution at rotation rates of 1200 rpm with a sweep rate of 5 mV s^{-1}.

Note 1 Synthesis of Fe−N−C catalysts

Briefly, taking the Fe−N−C catalysts derived from EDTA−Fe(II) as an example, the chelate of EDTA−Fe(II) monomer was prepared by the mixture of solution of EDTA-Na_2 and $FeSO_4 \cdot 7H_2O$ in the round-bottom flask in N_2 atmosphere (40°C water-bath). Here, please notice that a dropwise addition of EDTA-Na_2 solution to fully boiled $FeSO_4$ solution is recommended. Once the color of the mixture changed to dark green, dried it at 50 ^{o}C in the vacuum oven overnight. Then the high-quality EDTA−Fe(II) chelate powder was obtained followed by ball-milling. Afterward, the dark powder thus produced by temperature-programmed carbonation to 700 to 900 ℃ under N_2 atmosphere (5 ℃/min), held for 4 h, and cooled down to room temperature. Finally, to remove unstable phases and inorganic impurities, the pyrolyzed product was washed in H_2SO_4 solution, ethanol and DI water in sequence, and dried at 80 ℃ for 6 h. The resulting black powders are designated as Fe−N−C−x, where x represents the final pyrolysis temperature. Similarly, the other two kinds of Fe−N−C catalysts as control samples can be also prepared as mentioned above, but differed in the synthesis of specific chelates with corresponding precursors.

Note 2 Characterizations

The crystal structure of sample was characterized by powder X-ray diffraction (XRD) measurements (Bruker D8 Advance) between 10° and 90° at a scan step of $10^{o}\cdot min^{-1}$ operating at 40 kV and 30 mA using Cu Ka radiation. Morphology information was investigated by TEM observation using a high-resolution TEM/STEM H-800 (Hitachi, Japan) at an accelerating voltage of 220 kV. Energy-dispersive X-ray spectrum (EDX) was analyzed by an energy dispersive spectroscopy analyzer attached to the HRTEM. The XPS data were performed with an AXIS-Ultra instrument (Kratos Analytical, UK) using monochromatic Al Ka radiation (225 W, 15 mA, 15 kV), where the binding energy was calibrated against reference of C1s peak at 284.8 eV. Raman spectra were recorded on a microscopic confocal Raman spectrometer (JY Lab Raman HR 800) with an excitation laser source of 785 nm. The BET surface area was deduced from an analysis of the isotherm in the relative pressure range of 0.04−0.20. The total pore volume was calculated from the amount of nitrogen adsorbed at a relative pressure of 0.90. FTIR measurements were performed on catalysts mechanically mixed with KBr and pressed. IR spectra were collected in air at 2 cm^{-1} resolution on a Bruker Equinox 55 FTIR spectrophotometer, equipped with a MCT (Mercury Cadmium Telluride) detector. Fe K-edge X-ray absorption fine structure spectroscopy (XAFS) spectra were collected on beamline 1W1B at Beijing Synchrotron Radiation Facility. The ring storage energy of the synchrotron radiation accelerator during data collection was 2.5 GeV with current intensity of 50 mA. Fe K-edge spectrum of the sample was collected using transmission mode. Fe foil, FeO, Fe_3O_4 and Fe_2O_3 NPs were used as standard compounds. The tested samples of Fe-N-C catalysts were motor homogenized and pressed into thin slices with diameter of 10 mm and thickness of 2 mm. Athena software was used to process the normalization

and liner combination fitting (LCF) of the XANES spectra. Room-temperature ^{57}Fe Mössbauer spectra were recorded by using a Topologic 500A spectrometer and a proportional counter. ^{57}Co(Rh) moving with a constant acceleration mode was used as the γ-ray radioactive source. The velocity was calibrated by a standard α-iron foil. All spectra were computer-fitted to a Lorentzian shape with a least-squares fitting procedure. The isomer shifts (IS) were given with respect to the centroid of α-Fe at room temperature. The absorbers were obtained by pressing the powdered samples (about 10 mg/cm^2 of natural iron).

Note 3 TGA-MS analysis

Thermo-gravimetric analysis (TGA) was further performed to provide an estimate with regards to the composition of the synthesized Fe−N−C catalysts and to predict their formation process. The Fe−EDTA precursor was heated in N_2 under a temperature programming rate of 10 $^{o}C \cdot min^{-1}$, and the corresponding TGA curve was collected (Figure S11a), meanwhile the MS signals of generated gas were also detected (Figure S11b). The TGA results showed three weight loss steps in the following temperature ranges: 200-250, 325-400, and 750-900 ^{o}C, which are also consistent with the appearance of DTG peaks. The gradual decrease in weight with loss value of 10 % from 25 to 250 ^{o}C can be ascribed to the elimination of surface capping groups such as some volatile or decomposable of carbonic oxides (m/z = 28 and 44) from organic components and adsorbed water. While a pronounced weight loss of 17% was found in the temperature range of 325-400 ^{o}C with mass gas evolution of CO_2 (m/z = 44), CO (m/z = 28), H_2O (m/z = 18), NH_3 (m/z = 17) and NO (m/z = 30). It is clear that the separation of oxygen from Fe-EDTA source via the burn off of carbon and the decomposition of nitrogen was dominant, suggesting a reorganization of original carbon atom configuration, which agrees well with the Raman and FTIR results. Moreover, the predominant weight-loss of 25% was observed coupled only with the measure MS signal of CO gas in this temperature region, indicating a further decrease in weight throughout by removing oxygen and carbon from Fe−N−C−700 to Fe−N−C−900 catalysts. The continuous extraction of O by virtue of C atom, no longer N atom, not only led to a more abundant amorphous

structure on Fe−N−C−900 than Fe−N−C−800 (agree with the BET analysis), but also reveals the strong interaction of N−O and N−C bonds in the molecular structure of Fe−N−C catalysts in high temperature. Thus it can be seen that the Fe−N−C catalysts were probably developed via the stripping of O from the organic precursor Fe−EDTA, being helped by C atom at large, resulting in the rearrangement of Fe and N atoms residues on carbon matrix.

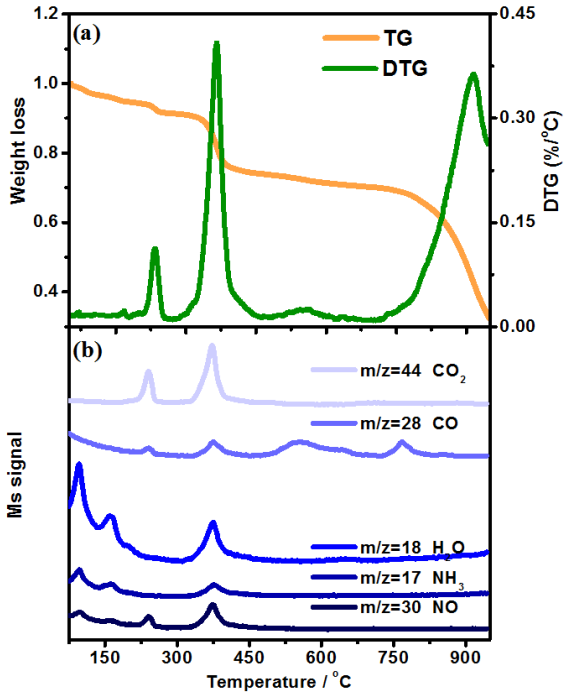

Figure S12. TGA-MS of Fe−N−C−800 catalysts; the Fe−EDTA was heated from 30 to 1000 ^{o}C under N_2, heat rate: 10 ^{o}C/min

Note 4 Computational model and details

Gibbs free energy calculations. The popular B3LYP (Becke, three-parameter, Lee-Yang-Parr) exchange-correlation hybrid density functional theory of Gaussian 03 was employed with a basis set of 6-31G (d,p).[1, 2] The unstrict polarization setting was used to calculate the breaking and forming of the chemical bond. [3] Seven different iron-nitrogen-carbon or iron nitride models were constructed referred to the literatures

and standard inorganic crystal structure information.[4-7] The edges of the carbon matrix are terminated by hydrogen atoms. The structures were relaxed until residual force on each atom is 0.01 eV/Å or less.

The ORR processes were simulated beginning with the adsorption of OOH on catalysts as an intermediate via the one-electron transfer, in which process the O_2 can adsorb an H^+ to form H^+–O–O, being simplified as OOH due to the charge neutral environment. After that, driving by the ionization potentials, the adsorbed H^+ of OOH could be easily divorced. The one-electron transformation reactions were simulated by keeping introducing H atoms via different structure models, which the optimization structures were obtained, and each adsorption energy for these molecules was calculated. The adsorption energy is defined as the energy difference between the adsorption and the isolated systems. Here, the energy of the isolated system refers to sum of energies of fore-step adsorbed molecules and the individual isolated adsorbate molecules. Thus, negative adsorption energy indicates that the adsorbate molecules would be energetically favorable to be adducted to the surface of the modeling structures.

Table S1. Impedance parameters of the Fe−N−C catalysts deduced from the equivalent circuit model of Nyquist plot

Catalysts	R_S (Ω mg)	R_{ct} (Ω mg)	*CPE-T* (μF mg^{-1})	*n*	*W* (Ω^{-1} mg^{-1})
Fe−N−C−700	0.039	475.30	0.0169	0.90	1618.62
Fe−N−C−800	0.041	88.23	0.0265	0.94	783.45
Fe−N−C−900	0.049	49.71	0.0575	0.93	160.17

Table S2 Calculation of parameters derived from the K-L plot of Fe−N−C−700, Fe−N−C−800 and Fe−N−C−900.

Catalysts	Potential	Slope	Intercept	n	J_k
Fe−N−C−700	-0.4	2.16115	0.22408	4.17	4.46
	-0.45	2.13272	0.21	4.20	4.76
	-0.5	2.17389	0.20076	4.17	4.98
	-0.55	2.11305	0.19187	4.22	5.21
	-0.6	2.07252	0.1912	4.38	5.23
	-0.65	2.05516	0.18979	4.42	5.27
	Average			4.2	5.0
Fe−N−C−800	-0.4	2.53704	0.05536	3.58	18.06
	-0.45	2.50908	0.05504	3.62	18.17
	-0.5	2.48602	0.04831	3.65	20.70
	-0.55	2.48641	0.05099	3.65	19.61
	-0.6	2.40059	0.0513	3.78	19.49
	-0.65	2.33943	0.049	3.88	20.41
	Average			3.7	19.4
Fe−N−C−900	-0.4	1.91546	0.24659	4.74	4.16
	-0.45	1.95569	0.22693	4.64	4.41
	-0.5	1.9271	0.21843	4.71	4.58
	-0.55	1.90854	0.21067	4.75	4.75
	-0.6	1.91306	0.20299	4.76	4.93
	-0.65	1.93524	0.19406	4.68	5.15
	Average			4.7	4.64

Table S3 Schematic diagrams of coordination and space structures of Fe, N and C atoms

Coordination	Molecular Structure (Up view)	Molecular Structure (Side view)	Structural Diagram (Side view)	Reference
$Fe^{II}N_4$, distorted (low-spin state, S=0 or 1)	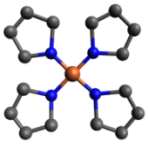	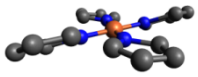	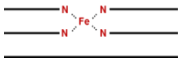	8
$Fe^{II}N_4$ centers, in-plane (low-spin state, S=0 or 1)	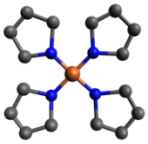	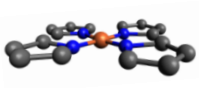	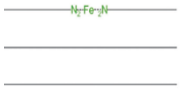	9
$Fe^{II}N_{2+2}$/C (Intermediate spin, S=1)	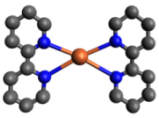	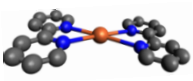	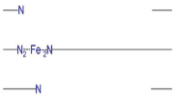	8, 10
N-$Fe^{II}N_{2+2}$...N_{prot}/C (High spin state, S=2)	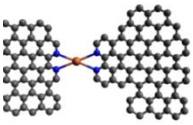	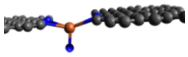	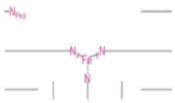	8, 11, 12
FeN_4C_8	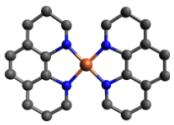	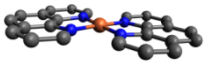		13
FeN_4C_{10}	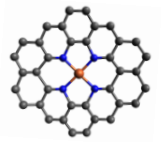	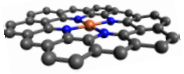		7
FeN_4C_{12}	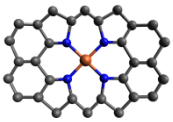	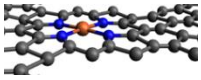		14

Table S4 Curve fitting results of Fe−N−C catalysts derived from EDTA−Fe(II) for EXAFS

Catalysts	Shell	CN	R (Å)	σ^2 (Å^2)	R factor (%)
Fe−N−C−700	Fe-N	11.64	1.99	0.01390	0.48
	Fe-Fe	3.41	2.81	0.02430	
Fe−N−C−800	Fe-N	11.31	2.00	0.01312	0.30
	Fe-Fe	2.80	2.83	0.02132	
Fe−N−C−900	Fe-N	11.14	1.99	0.01225	0.29
	Fe-Fe	3.05	2.86	0.02141	
Fe-N Reference	Fe-N	2.00	1.93	--	--
	Fe-Fe	6.00	2.67	--	

Table S5 Curve fitting results of Fe−N−C catalysts derived from EDDA−Fe(II) and phenanthroline−Fe(II) for EXAFS

Catalysts	Shell	CN	R (Å)	σ^2 (Å^2)	R factor (%)
Phenanthroline−Fe(II)-derivative Fe−N−C catalyst	Fe-N	11.64	1.95	0.01390	0.48
	Fe-Fe	3.41	2.69	0.02430	
EDDA-derivative Fe−N−C catalyst	Fe-N	11.31	2.12	0.01312	0.30
	Fe-Fe	2.80	2.86	0.02132	

Reference

1. Sharma, S.; Ganguly, A.; Papakonstantinou, P.; Miao, X. P.; Li, M. X.; Hutchison, J. L.; Delichatsios, M.; Ukleja, S. Rapid Microwave Synthesis of CO Tolerant Reduced Graphene Oxide-Supported Platinum Electrocatalysts for Oxidation of Methanol. *J Phys Chem C* 2010, 114, 19459-19466.

2. Wang, S. Y.; Yu, D. S.; Dai, L. M. Polyelectrolyte Functionalized Carbon Nanotubes as Efficient Metal-free Electrocatalysts for Oxygen Reduction. *Journal of the American Chemical Society* 2011, 133, 5182-5185.

3. Wang, Y. X.; Balbuena, P. B. Ab initio molecular dynamics simulations of the oxygen reduction reaction on a Pt(111) surface in the presence of hydrated hydronium (H3O)(+)(H2O)(2): Direct or series pathway? *Journal of Physical Chemistry B* 2005, 109, 14896-14907.

4. Jiang, W. J.; Gu, L.; Li, L.; Zhang, Y.; Zhang, X.; Zhang, L. J.; Wang, J. Q.; Hu, J. S.; Wei, Z.; Wan, L. J. Understanding the High Activity of Fe-N-C Electrocatalysts in Oxygen Reduction: Fe/Fe3C Nanoparticles Boost the Activity of Fe-N(x). *J Am Chem Soc* 2016, 138, 3570-8.

5. Tylus, U.; Jia, Q.; Strickland, K.; Ramaswamy, N.; Serov, A.; Atanassov, P.; Mukerjee, S. Elucidating Oxygen Reduction Active Sites in Pyrolyzed Metal-Nitrogen Coordinated Non-Precious-Metal Electrocatalyst Systems. *The journal of physical chemistry. C, Nanomaterials and interfaces* 2014, 118, 8999-9008.

6. Deng, J.; Ren, P.; Deng, D.; Bao, X. Enhanced electron penetration through an ultrathin graphene layer for highly efficient catalysis of the hydrogen evolution reaction. *Angew Chem Int Ed Engl* 2015, 54, 2100-4.

7. Zitolo, A.; Goellner, V.; Armel, V.; Sougrati, M. T.; Mineva, T.; Stievano, L.; Fonda, E.; Jaouen, F. Identification of catalytic sites for oxygen reduction in iron- and nitrogen-doped graphene materials. *Nat Mater* 2015, 14, 937-42.

8. Kramm, U. I.; Herranz, J.; Larouche, N.; Arruda, T. M.; Lefevre, M.; Jaouen, F.; Bogdanoff, P.; Fiechter, S.; Abs-Wurmbach, I.; Mukerjee, S.; Dodelet, J. P. Structure of the catalytic sites in Fe/N/C-catalysts for O2-reduction in PEM fuel cells. *Physical chemistry chemical physics : PCCP* 2012, 14, 11673-88.

9. Koslowski, U. I.; Abs-Wurmbach, I.; Fiechter, S.; Bogdanoff, P. Nature of the Catalytic Centers of Porphyrin-Based Electrocatalysts for the ORR: A Correlation of Kinetic Current Density with the Site Density of Fe−N4Centers. *The Journal of Physical Chemistry C* 2008, 112, 15356-15366.

10. Melendres, C. A. Moessbauer and Raman spectra of carbon-supported iron phthalocyanine. *The Journal of Physical Chemistry* 1980, 84, 1936-1939.

11. Collman, J. P.; Hoard, J. L.; Kim, N.; Lang, G.; Reed, C. A. Synthesis, stereochemistry, and structure-related properties of alpha, beta, gamma, delta-tetraphenylporphinatoiron(II). *J Am Chem Soc* 1975, 97, 2676-81.

12. Collman, J. P.; Gagne, R. R.; Reed, C. A.; Halbert, T. R.; Lang, G.; Robinson, W. T. "Picket fence porphyrins." Synthetic models for oxygen binding hemoproteins. *J Am Chem Soc* 1975, 97, 1427-39.

13. Kramm, U. I.; Lefevre, M.; Bogdanoff, P.; Schmeisser, D.; Dodelet, J. P. Analyzing Structural Changes of Fe-N-C Cathode Catalysts in PEM Fuel Cell by

Mossbauer Spectroscopy of Complete Membrane Electrode Assemblies. *J Phys Chem Lett* 2014, 5, 3750-6.
14. Herranz, J.; Jaouen, F.; Lefevre, M.; Kramm, U. I.; Proietti, E.; Dodelet, J. P.; Bogdanoff, P.; Fiechter, S.; Abs-Wurmbach, I.; Bertrand, P.; Arruda, T. M.; Mukerjee, S. Unveiling N-protonation and anion-binding effects on Fe/N/C-catalysts for O2 reduction in PEM fuel cells. *The journal of physical chemistry. C, Nanomaterials and interfaces* 2011, 115.